

Analysis of the Crouzeix-Raviart Surface Finite Element Method for vector-valued Laplacians

Carolin Mehlmann*

November 21, 2024

Abstract

Recently a nonconforming surface finite element was developed to discretize 3D vector-valued compressible flow problems arising in climate modeling. In this contribution we derive an error analysis for this approach on a vector-valued Laplace problem, which is an important operator for fluid-equations on the surface. In our setup, the problem is approximated via edge-integration on local flat triangles using the non-conforming linear Crouzeix-Raviart element. The latter is continuous at the edge midpoints in each vector component. The developed Crouzeix-Raviart approximation is a non-parametric approach that works on local coordinate systems, established in each triangle. This setup is numerically efficient and straightforward to implement. For this Crouzeix-Raviart discretization we derive optimal error bounds in the H^1 -norm and L^2 -norm and present an estimate for the geometric error. Numerical experiments validate the theoretical results.

1 Introduction

Low order nonconforming finite element discretizations play an important role for the approximation of geophysical flow problems on the surface of the Earth [24, 6]. On the used meshes in climate models this type of discretization is a good compromise between accuracy and efficiency of the numerical setup [25, 23, 6]. The analysis of a nonconforming finite element discretization for the vector-valued surface Laplace, which forms an essential part of fluid equations in climate applications, is the topic which is treated in this paper.

In the last years there is an increasing interest in the analysis of finite elements for surface fluid equations, e.g. [1, 26, 12, 16, 3, 4, 17, 21, 29]. Considering the error analysis most works focus on viscous surface flows. Several papers derive error bounds for finite element discretizations of the surface Stokes problem [28, 27, 17, 14, 2, 8, 5]. The majority of authors consider H^1 -conforming finite

*Institute of Analysis and Numerics, Otto-von-Guericke University Magdeburg, Universitätsplatz 2, 39106 Magdeburg, Germany, carolin.mehlmann@ovgu.de

elements and weakly enforce the tangentiality of the velocity field by a Lagrange multiplier or a penalty method [28, 27, 17, 14]. Other approaches give up the H^1 -conformity, but realize the tangentiality by construction of the elements [2, 8]. A third option studied in the literature are surface finite elements based on stream functions [5].

An important aspect in the analysis of finite element methods for flow problems on surfaces is to ensure that the numerical approximation of the flow is tangential to the surface. This difficulty already arises in the analysis of the surface Laplace equation. Vector-valued Laplace problems on the surface are easier to analyze than the Stokes problem because the equation consists only of the velocity vector and no pressure unknown. Therefore, the vector-valued Laplace equations are a useful simplification of more complex surface flow problems for the finite element analysis. In the work of [10, 18, 12, 15] finite element methods are studied for a surface vector Laplace problem and optimal error bounds are derived. The tangentiality condition of the vector-valued velocity field is enforced either by a penalty term or a Lagrange multiplier.

In this paper we analyze a recently developed nonconforming Crouzeix-Raviart approximation [24] for the surface Laplace equation, which has been also studied in [22]. The nonconforming discretization has been developed for an approximation of the sea-ice dynamics in the climate model ICON [19]. In the ICON model the coupled systems of equations are discretized in local coordinate systems based on flat instead of curved mesh elements (triangles). A similar approximation has been applied to discretize the scalar valued shallow water equation [6]. The usage of flat instead of curved mesh elements introduces a geometrical error. In this setup the error coming from the geometry is balanced with the first order approximation of the nonconforming finite element. This aspect has been analyzed for the scalar Laplace problem in [11]. In this contribution we derive an analysis for a vector-valued Laplacian based on covariant derivatives of the tangential fields. The problem includes the numerical treatment of the tangential condition of the velocity field. We will present an error analysis for the numerical approach described in [24].

The main contributions of the paper are the following. We derive a finite element variational formulation of the problem as well as a-priori error estimates. The derivation shows optimal error bounds and presents an estimate for the geometrical error. The theoretical findings are validated with numerical results.

The considered Crouzeix-Raviart approach is very different to other vector-valued finite element approximations on the surface. The method does not need an extra condition to enforce the tangentiality of the velocity field as it is common in many other approaches cited above. By construction the discrete velocity field is always in the corresponding tangential plane. Unlike other penalty free surface elements [8], which discretize the incompressible Stokes equation with $H^1(\text{div})$ -conforming finite elements, we consider the Crouzeix-Raviart approach as a nonconforming finite element in the H^1 -setting with the aim to apply the discretization to compressible non saddle-type fluid problems as in [24]. The finite elements studied in [8] are H^1 -nonconforming nodal elements. However the error analysis derived in the paper of [8] does not present an L^2 -

estimate, which is given in our contribution.

We address the problem in the context of surface finite elements (SFEM), where the surface is approximated by a geometry Γ_h , usually a polyhedron.

In case of the $H^1(\text{div})$ conforming approach a finite element function is set up via a Piola transformation in each triangle of the polyhedron. In contrast to that, we establish in each face of the polyhedron a local basis and express the Crouzeix-Raviart approximation in terms of the conormal vectors \mathbf{n}_E, τ_E given in the edge midpoint. While τ_E is continuous, \mathbf{n}_E is discontinuous along an edge. Therefore, the approximation is discontinuous along edges. A sketch of the setting is shown in Figure 1. The discretization is straightforward to implement and benefits from its efficiency, see for instance [23].

The paper is structured as follows. Section 2 presents the vector-valued Laplace problem and introduces the surface derivatives. The nonconforming Crouzeix-Raviart approach is outlined in Section 3. The error analysis is carried out in Section 4. The main results of the section are the optimal error bounds in H^1 -norm and L^2 -norm. Numerical examples to validate the theoretical results are presented in Section 5.

2 Preliminaries

2.1 Surface, derivatives and norms

We consider a oriented, connected, C^∞ smooth surface Γ in \mathbb{R}^3 with $\partial\Gamma = \emptyset$. The signed distance function of Γ is given by $d(x)$. Using the distance function we define the unit outward pointing normal vector as

$$\mathbf{n}(x) = \nabla d(x), \quad (1)$$

where ∇ is the standard gradient in \mathbb{R}^3 . We introduce a neighborhood, a strip around Γ with distance δ , as

$$U = \{x \in \mathbb{R}^3 : \text{dist}(x, \Gamma) \leq \delta\}, \quad (2)$$

where $\text{dist}(x, \Gamma)$ is the Euclidean distance between x and Γ . Let δ be small enough such that a unique closest point mapping $p(x)$ from $U \rightarrow \Gamma$ exists with

$$p(x) = x - d(x)\mathbf{n}(p(x)). \quad (3)$$

Let $\phi : \Gamma \rightarrow \mathbb{R}$ with $\tilde{\phi} : U \rightarrow \mathbb{R}$ we denote the extension to the neighborhood U , defined along the normal directions as

$$\tilde{\phi}(x) = \phi(p(x)), \quad \forall x \in U. \quad (4)$$

Later on Γ_h will denote the discrete surface which is defined by the triangulation and Γ will represent the lifted counterpart. The usage will be clear from the given context. Analogously the lift of a function $\phi : \Gamma_h \rightarrow \mathbb{R}$ on $\Gamma_h \subset U$ to Γ is given as

$$\phi^l(x) = \phi(\eta(x)), \quad \forall x \in \Gamma, \quad (5)$$

where $\eta(x)$ is the unique solution of

$$x = p(\eta) = \eta - d(\eta)n(x). \quad (6)$$

Throughout the paper, we apply a component-wise lifting and extension of vector-valued functions. To define the surface derivatives we introduce the projection into the tangential plane as

$$\mathbf{P} = \mathbf{I} - \mathbf{n}\mathbf{n}^T, \quad \mathbf{P} = (\mathbf{P}^{ij}), \quad i, j = 1, \dots, 3. \quad (7)$$

The covariant derivatives of a vector field $\tilde{\mathbf{v}}$ are defined as

$$\nabla_\Gamma \mathbf{v} := \mathbf{P} \nabla \tilde{\mathbf{v}} \mathbf{P}. \quad (8)$$

Similar to [10] we introduce the divergence operator for vector-valued $\tilde{\mathbf{v}} : \Gamma \rightarrow \mathbb{R}^3$ and matrix valued objects $A : \Gamma \rightarrow \mathbb{R}^3 \times \mathbb{R}^3$ as

$$\begin{aligned} \operatorname{div}_\Gamma \mathbf{v} &= \operatorname{tr}(\nabla_\Gamma \mathbf{v}) = \operatorname{tr}(\mathbf{P} \nabla \tilde{\mathbf{v}} \mathbf{P}), \\ \operatorname{div}(A) &:= \left(\operatorname{div}_\Gamma(\mathbf{e}_1^T A), \operatorname{div}_\Gamma(\mathbf{e}_2^T A), \operatorname{div}_\Gamma(\mathbf{e}_3^T A) \right), \end{aligned}$$

where $\mathbf{e}_1, \mathbf{e}_2, \mathbf{e}_3$ are the unit vectors of \mathbb{R}^3 . The surface Laplacian is defined by

$$\Delta_\Gamma \mathbf{v} := \mathbf{P} \operatorname{div}_\Gamma(\nabla_\Gamma \mathbf{v}).$$

This is the so called Bochner Laplace, which is also treated in [13]. In differential geometry and in exterior calculus a different Laplace operator, the Hodge Laplace, is considered. Another surface Laplace operator based on the symmetric gradient $\nabla \mathbf{v} + \nabla \mathbf{v}^T$ is analyzed in [10].

Let $\omega \subset \Gamma$. In the following, we introduce the surface Sobolev space of k times weakly differentiable vector valued functions with componentwise derivatives and the corresponding norm as

$$\|\mathbf{v}\|_{H^k(\omega)}^2 := \sum_{j=0}^k \|(\nabla \mathbf{P})^j \tilde{\mathbf{v}}\|_{L^2(\omega)}^2, \quad |\mathbf{v}|_{H^k(\omega)}^2 := \|(\nabla \mathbf{P})^k \tilde{\mathbf{v}}\|_{L^2(\omega)}^2, \quad (9)$$

where $\omega \subset \Gamma$. We write $H^k(\Gamma) := \left(H^k(\Gamma) \right)^3$ for vector-valued functions in \mathbb{R}^3 . The space of the vector-valued functions that are tangential to the surface is named as

$$H_{tan}^k(\Gamma) := \{\mathbf{v} \in H^k(\Gamma) | \mathbf{v} \cdot \mathbf{n} = 0\}. \quad (10)$$

2.2 Model problem

The vector-valued problem based on the Bochner Laplace is given as

$$-\mathbf{P} \operatorname{div}_\Gamma(\nabla_\Gamma \mathbf{u}) + \mathbf{u} = \mathbf{f}, \quad (11)$$

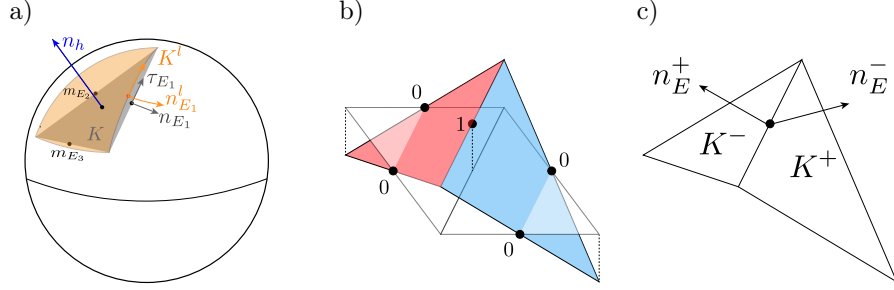


Figure 1: a) The tangential plane which coincides with the sphere at the vertices of the triangle. The outward pointing normal vector is named \mathbf{n}_h . The tangential and conormal of the flat triangle K (shaded in grey) to an edge E is called \mathbf{n}_E, τ_E . Accordingly the tangential and conormal of the curved triangle K^l is named \mathbf{n}_E^l, τ_E^l . b) Crouzeix-Raviart basis function. c) The outward pointing conormal vectors \mathbf{n}_E^\pm that share an edge E .

where the zero order term \mathbf{u} has been added to the left hand side of the equation to avoid technical details related to the kernel of the Laplace operator. The corresponding weak formulation reads as:

$$\text{Find } \mathbf{u} \in H_{tan}^1(\Gamma) \text{ s.t. } a(\mathbf{u}, \mathbf{v}) = l(\mathbf{v}), \forall \mathbf{v} \in H_{tan}^1(\Gamma), \quad (12)$$

with $a(\mathbf{v}, \mathbf{u}) = (\nabla_\Gamma \mathbf{u}, \nabla_\Gamma \mathbf{v})_\Gamma + (\mathbf{u}, \mathbf{v})_\Gamma$, $\mathbf{u}, \mathbf{v} \in H_{tan}^1(\Gamma)$ and $l(\mathbf{v}) = (\mathbf{f}, \mathbf{v})_\Gamma$, where (\cdot, \cdot) is the standard L^2 -inner product and $\mathbf{f} \in H_{tan}^{-1}(\Gamma)$. The Bochner-Laplace equation is analyzed in [12]. In the study the authors demonstrated by the Lax-Milgram theorem the uniqueness of the solution of equation (12) and derive the following regularity estimates

$$\|\mathbf{u}\|_{H_{tan}^2(\Gamma)} \leq c \|\mathbf{f}\|_{L^2(\Gamma)}, \quad (13)$$

where c is a generic positive constant.

3 The nonconforming finite element approximation on the surface

We denote by $\Gamma_h = \cup_{i \in \mathbb{N}} K_i \subset U$ the triangulation of Γ . The triangulation is shape regular and quasi uniform with the maximal diameter $h = \max_{K \in \Gamma_h} \text{diam}(K)$. The triangulation is made such that all vertices \mathbf{x} lie on Γ . Each triangle K consists of three vertices $\mathbf{x}_1, \mathbf{x}_2, \mathbf{x}_3$ numbered counter clockwise and edges $E_1 = (\mathbf{x}_1, \mathbf{x}_2), E_2 = (\mathbf{x}_2, \mathbf{x}_3), E_3 = (\mathbf{x}_3, \mathbf{x}_1)$. Based on the vectors $\vec{E}_1 = \mathbf{x}_2 - \mathbf{x}_1, \vec{E}_2 = \mathbf{x}_3 - \mathbf{x}_2, \vec{E}_3 = \mathbf{x}_1 - \mathbf{x}_3$ the outward pointing normal vector is calculated

by

$$\mathbf{n}_h^K = \frac{\vec{E}_1 \times (-\vec{E}_3)}{\|\vec{E}_1 \times (-\vec{E}_3)\|}.$$

Using \mathbf{n}_h^K the projection onto the tangent space of Γ_h is defined by

$$\mathbf{P}_h = \mathbf{I} - \mathbf{n}_h^K (\mathbf{n}_h^K)^T. \quad (14)$$

The setup is visualized in the left panel of Figure 1. The conormal vectors to an edge E_i , $i = 1, \dots, 3$ is given by

$$\tau_{E_i}^K = \frac{\vec{E}_i}{\|\vec{E}_i\|}, \quad \mathbf{n}_{E_i}^K = \tau_{E_i}^K \times \mathbf{n}_h^K, \quad i = 1, 2, 3.$$

To any $K \in \Gamma_h$ a curved triangle $K^l = p(K)$ on Γ is related such that the set of curved triangular faces is defined as $\Gamma_h^l = \{K^l : K \in \Gamma_h\}$ with $\Gamma = \cup_{K^l \in \Gamma_h^l} K^l$. Any edge midpoint m_E of edge E is shared by two triangles K^+ and K^- . We denote the outward pointing conormal vectors by \mathbf{n}_E^\pm . The conormal vectors of a curved edge $E^l = p(E)$ are named $\mathbf{n}_{E^l}^\pm, \tau_{E^l}^\pm$. A sketch of the setup is shown in the right panel of Figure 1.

3.1 The Crouzeix-Raviart Finite Element space

To introduce the Crouzeix-Raviart functions we consider a uniform reference triangle \hat{K} with edges of length 1. \hat{K} is related to each $K \in \Gamma_h$ via an affine linear mapping $F_K : \hat{K} \rightarrow K$. In each edge midpoint $m_{\hat{E}_i}$, with $i = 1, 2, 3$ of the reference triangle \hat{K} the linear Crouzeix-Raviart basis functions are given by the defining properties

$$\hat{\phi}_i \in P^1(\hat{K}), \quad \hat{\phi}_i(m_{\hat{E}_j}) = \delta_{ij}, \quad \forall i, j = 1, \dots, 3.$$

$$\text{Hence,} \quad \int_{\hat{E}_j} \hat{\phi}_i d\hat{s} = \delta_{ij}, \quad \forall i, j = 1, \dots, 3.$$

Based on this properties it holds that

$$\Rightarrow \quad \partial_{\mathbf{n}_{E_i}} \phi_i(m_{E_i}) = \frac{2}{h_i}, \quad \partial_{\tau_{E_i}} \phi_i(m_{E_i}) = 0, \quad \forall i = 1, \dots, 3,$$

where h_i is the triangles height on edge E_i . Using the basis functions we indicate a finite element function locally by its conormal components in the planes spanned by each element K

$$\mathbf{V}_K := \text{span}(\mathbf{n}_{E_i}^K \phi_i^K, \tau_{E_j}^K \phi_j^K, i, j = 1, 2, 3), \quad (15)$$

where $\phi_i^K = \hat{\phi}_i \circ F_K^{-1}$. Thus, we get

$$\begin{aligned} \mathbf{u}_h|_K &= \sum_{i=1}^3 (u_i^{n,K} \mathbf{n}_{E_i}^K + u_i^{t,K} \tau_{E_i}^K) \phi_i^K, \\ \nabla \mathbf{u}_h|_K &= \sum_{i=1}^3 (u_i^{n,K} \mathbf{n}_{E_i}^K + u_i^{t,K} \tau_{E_i}^K) (\nabla \phi_i^K)^T \\ &= \sum_{i=1}^3 (u_i^{n,K} \mathbf{n}_{E_i}^K + u_i^{t,K} \tau_{E_i}^K) \left((\mathbf{n}_{E_i}^K)^T \partial_{\mathbf{n}_{E_i}} \phi_i^K + (\tau_{E_i}^K)^T \underbrace{\partial_{\tau_{E_i}} \phi_i^K}_{=0} \right), \end{aligned}$$

where $u^{n,K}$, $u^{t,K}$ are the scalar normal and tangential coefficients, respectively. To improve the readability will neglect the superscript K in the following. The global space of this vectors is given by

$$\bar{\mathbf{V}}_h = \left\{ \mathbf{v} : \Gamma_h \rightarrow \mathbb{R}^3, \mathbf{v}|_K \in \mathbf{V}_K \right\},$$

whereas the space of the tangential Crouzeix-Raviart functions on Γ_h is introduced as

$$\begin{aligned} \mathbf{V}_h = \left\{ \mathbf{v} \in \bar{\mathbf{V}}_h, \mathbf{v}|_K \in \mathbf{V}_K, \quad \forall E = \partial K^+ \cap \partial K^- \ (K^+ \neq K^-) : \right. \\ \left. \mathbf{v}|_{K^+}(m_E) \cdot \mathbf{n}_E^+ = -\mathbf{v}|_{K^-}(m_E) \cdot \mathbf{n}_E^-, \right. \\ \left. \mathbf{v}|_{K^+}(m_E) \cdot \tau_E^+ = -\mathbf{v}|_{K^-}(m_E) \cdot \tau_E^- \right\}. \quad (16) \end{aligned}$$

The tangential condition of the vector fields of (16) are fulfilled by construction. The coupling of two Crouzeix-Raviart basis functions on two neighboring elements is shown in the middle panel in Figure 1. The jump of a vector-valued function across an edge E is defined as

$$[\mathbf{v}] = \lim_{s \rightarrow 0_+} \left(\mathbf{v}(x - s\mathbf{n}_E^+) - \mathbf{v}(x - s\mathbf{n}_E^-) \right). \quad (17)$$

The condition formulated in (16) yields the continuity of vector components at the edges midpoints. Thus, the average over the normal and the tangential component is zero and we get that $\int_E [\mathbf{v}_h \mathbf{n}_E] = 0$ and $\int_E [\mathbf{v}_h \tau_E] = 0$. The discrete vector-valued derivative for any $\mathbf{v}_h \in \mathbf{V}_h$ is defined as

$$\nabla_{\Gamma_h} \mathbf{v}_h = \mathbf{P}_h(x) \nabla \mathbf{v}_h(x) \mathbf{P}_h(x), \quad x \in \Gamma_h. \quad (18)$$

3.2 Formulation of the Method

The discrete analog to (12) reads as:

$$\text{Find } \mathbf{u}_h \in \mathbf{V}_h \text{ s.t. } a_h(\mathbf{u}_h, \mathbf{v}_h) = l_h(\mathbf{v}_h) \quad \forall \mathbf{v}_h \in \mathbf{V}_h, \quad (19)$$

with the bilinear form and the linear functional

$$a_h(\mathbf{u}_h, \mathbf{v}_h) = \sum_{K \in \Gamma_h} (\nabla_{\Gamma_h} \mathbf{u}_h, \nabla_{\Gamma_h} \mathbf{v}_h)_K + (\mathbf{u}_h, \mathbf{v}_h)_{\Gamma_h}, \quad l_h(\mathbf{v}_h) = (\tilde{\mathbf{f}}, \mathbf{v}_h)_{\Gamma_h}. \quad (20)$$

The broken H^1 semi-norm is defined as

$$|\mathbf{v}_h|_{H^1(\Gamma_h)}^2 = \sum_{K \in \Gamma_h} \|\nabla_{\Gamma_h} \mathbf{v}_h\|_{L^2(K)}^2. \quad (21)$$

Based on the weak formulation, the energy norm is given by

$$\|\mathbf{v}_h\|_h^2 = |\mathbf{v}_h|_{H^1(\Gamma_h)}^2 + \|\mathbf{v}_h\|_{L^2(\Gamma_h)}^2 = a_h(\mathbf{v}_h, \mathbf{v}_h). \quad (22)$$

We note that $\|\mathbf{v}_h\|_h$ is a norm on \mathbf{V}_h . We state the following relationship between the vector-valued gradient and the Laplace operator. Applying Green's formula to the first term of $a_h(\mathbf{u}_h, \mathbf{v}_h)$ gives

$$\left(\nabla_{\Gamma_h} \mathbf{u}_h, \nabla_{\Gamma_h} \mathbf{v}_h \right)_K = - \left(\mathbf{P}_h \operatorname{div}_{\Gamma_h} (\nabla_{\Gamma_h} \mathbf{u}_h), \mathbf{v}_h \right)_K + \int_{\partial K} (\nabla_{\Gamma_h} \mathbf{u}_h) \mathbf{n}_E \cdot \mathbf{v}_h d\sigma. \quad (23)$$

The discrete variational formulation (19) is elliptic and continuous and therefore has a unique solution. The discrete problem introduces three nonconformities compared to the original formulation (12), namely the geometric error $\Gamma_h \neq \Gamma$, tangential inconsistency $\mathbf{P}_h \neq \mathbf{P}$ and the H^1 nonconformity.

4 A priori error estimates

Together with the geometric relations introduced in Section 2 and Section 3, the following geometric approximation holds true for our setup.

Lemma 4.1 (Geometry approximation). *Let $\Gamma_h \subset U$ be an approximation of Γ with properties outlined above. Assume that the mesh size h is small enough. Then it holds that*

$$\|\mathbf{P} - \mathbf{P}_h\| \leq ch, \quad (24)$$

$$\|\mathbf{n}_{E^l}^\pm - \mathbf{P} \mathbf{n}_E^\pm\| \leq ch^2. \quad (25)$$

Proof. The proof of (24)-(25) is given in Appendix A of [20]. \square

By the following bounds we relate the norms on Γ and Γ_h .

Lemma 4.2 (Norm equivalence). *Let $K \in \Gamma_h$ and $K^l \subset \Gamma$ its lifting. If $\mathbf{v} \in H^2(K^l)$, then it holds for any $K^l \subset \Gamma$ that*

$$\|\mathbf{v}\|_{L^2(K^l)} \leq c \|\tilde{\mathbf{v}}\|_{L^2(K)} \leq c \|\mathbf{v}\|_{L^2(K^l)}, \quad (26)$$

$$|\mathbf{v}|_{H^1(K^l)} \leq c |\tilde{\mathbf{v}}|_{H^1(K)} \leq c |\mathbf{v}|_{H^1(K^l)}, \quad (27)$$

$$|\tilde{\mathbf{v}}|_{H^2(K)} \leq c |\mathbf{v}|_{H^2(K^l)}, \quad (28)$$

$$|\mathbf{v}|_{H^2(K^l)} \leq c |\tilde{\mathbf{v}}|_{H^2(K)}. \quad (29)$$

Proof. The inequalities (26)-(27) are proven in [12] in Section 4.2. The inequalities (28) and (29) are proven for the scalar case in Appendix B of [20] and can be directly translated to the vector-valued setup. \square

Interpolation operator. We make use of the interpolation operator introduced by Crouzeix and Raviart in [7]. Let $K \subset \Omega_h$ and $\phi \in H^1(K^l)$. On K the Crouzeix-Raviart interpolation $\Pi_K \phi$ is defined as

$$(\Pi_K \phi)(m_{E_i}) = \frac{1}{|E_i|} \int_{E_i} \tilde{\phi} d\sigma_h, \forall \phi \in H^1(K^l), \quad (30)$$

where $|E_i|$ is the length of the edge E_i . The local interpolation estimate [7] is given by

$$\|\tilde{\phi} - \Pi_K \phi\|_{L^2(K)} + h|\tilde{\phi} - \Pi_K \phi|_{H^1(K)} \leq ch^2 |\tilde{\phi}|_{H^2(K)}, \quad (31)$$

where $\tilde{\phi} \in H^2(K)$. The global interpolation operator Π_h is defined as

$$(\Pi_h \phi)|_K = \Pi_K \phi, \forall K \in \Gamma_h.$$

Note that for a vector-valued function $\mathbf{v} \in H_{tan}^1(\Gamma)$ the component-wise extension is not in the discrete tangential space \mathbf{V}_h (16). Thus, we introduce a second interpolation $\Pi_h^{tan} : H_{tan}^1(\Gamma) \rightarrow \mathbf{V}_h$ with $\Pi_h^{tan}|_K \mathbf{v} = \Pi_K^{tan} \mathbf{v}$ with the following defining properties

$$\frac{1}{|E_i|} \int_{E_i} \Pi_h^{tan} \mathbf{v} \cdot \mathbf{n}_{E_i} d\sigma_h = \frac{1}{|E_i|} \int_{E_i} \tilde{\mathbf{v}} \cdot \mathbf{n}_{E_i} d\sigma_h, \quad (32)$$

$$\frac{1}{|E_i|} \int_{E_i} \Pi_h^{tan} \mathbf{v} \cdot \tau_{E_i} d\sigma_h = \frac{1}{|E_i|} \int_{E_i} \tilde{\mathbf{v}} \cdot \tau_{E_i} d\sigma_h. \quad (33)$$

This means that components with respect to Γ are interpolated into components with respect to K , see Figure 1 a) for an visualization.

Lemma 4.3 (Interpolation Estimates). *For $\mathbf{v} \in H_{tan}^1(\Gamma)$ the following interpolation error estimates hold*

$$\|\nabla_{\Gamma_h}(\tilde{\mathbf{v}} - \Pi_h^{tan} \mathbf{v})\|_{L^2(\Gamma_h)} \leq ch \|\tilde{\mathbf{v}}\|_{H^1(\Gamma_h)} \quad (34)$$

$$\|\mathbf{P}(\tilde{\mathbf{v}} - \Pi_h^{tan} \mathbf{v})\|_{L^2(\Gamma_h)} \leq ch^2 \|\tilde{\mathbf{v}}\|_{H^2(\Gamma_h)}, \quad (35)$$

and the in the energy norm we have

$$\|\tilde{\mathbf{v}} - \Pi_h^{tan} \mathbf{v}\|_h \leq ch \|\tilde{\mathbf{v}}\|_{H^2(\Gamma_h)}. \quad (36)$$

Proof. **Estimate (34)** is obtained by the following calculation:

$$\left\| \nabla_{\Gamma_h}(\tilde{\mathbf{v}} - \Pi_h^{tan} \mathbf{v}) \right\|_{L^2(K)} \leq \underbrace{\left\| \nabla_{\Gamma_h}(\tilde{\mathbf{v}} - \Pi_h \mathbf{v}) \right\|_{L^2(K)}}_{O(h), (31)} + \left\| \nabla_{\Gamma_h}(\Pi_h \mathbf{v} - \Pi_h^{tan} \mathbf{v}) \right\|_{L^2(K)}.$$

On each cell K we refer by ϕ_i , with $i = 1, 2, 3$ to the Crouzeix-Raviart basis functions. To bound $\|\nabla_{\Gamma_h}(\Pi_h \mathbf{v} - \Pi_h^{tan} \mathbf{v})\|_{L^2(K)}$ we express the two interpolations as

$$\Pi_h \mathbf{v}|_K = \sum_{i=1}^3 \phi_i \alpha_i(\tilde{\mathbf{v}}), \quad \alpha_i(\tilde{\mathbf{v}}) = \frac{1}{|E_i|} \int_{E_i} \tilde{\mathbf{v}} d\sigma_h, \quad (37)$$

and

$$\begin{aligned} \Pi_h^{tan} \mathbf{v}|_K &= \sum_{i=1}^3 \phi_i \alpha_i^{tan}(\tilde{\mathbf{v}}), \\ \alpha_i^{tan}(\tilde{\mathbf{v}}) &= \frac{1}{|E_i|} \int_{E_i} (\tilde{\mathbf{v}} \cdot \mathbf{n}_{E_i^l}) \cdot \mathbf{n}_{E_i} + \frac{1}{|E_i|} \int_{E_i} (\tilde{\mathbf{v}} \cdot \tau_{E_i^l}) \cdot \tau_{E_i} d\sigma_h. \end{aligned} \quad (38)$$

and use that $\nabla_{\Gamma_h} \mathbf{P}_h \Pi_h \mathbf{v} = \nabla_{\Gamma_h} \Pi_h \mathbf{v}$. Thus, we get

$$\begin{aligned} \left\| \nabla_{\Gamma_h} \left(\mathbf{P}_h (\Pi_h \mathbf{v} - \Pi_h^{tan} \mathbf{v}) \right) \right\|_{L^2(K)} &= \left\| \nabla_{\Gamma_h} \left(\mathbf{P}_h \left(\sum_{i=1}^3 \phi_i (\alpha_i(\tilde{\mathbf{v}}) - \alpha_i^{tan}(\tilde{\mathbf{v}})) \right) \right) \right\|_{L^2(K)} \\ &= \left\| \nabla_{\Gamma_h} \left(\sum_{i=1}^3 \phi_i \mathbf{P}_h (\alpha_i(\tilde{\mathbf{v}}) - \alpha_i^{tan}(\tilde{\mathbf{v}})) \right) \right\|_{L^2(K)} \\ &\leq \sum_{i=1}^3 \underbrace{\left\| \mathbf{P}_h (\alpha_i(\tilde{\mathbf{v}}) - \alpha_i^{tan}(\tilde{\mathbf{v}})) \right\|}_{(\star)} \underbrace{\left\| \nabla_{\Gamma_h} \phi_i \right\|_{L^2(K)}}_{\leq \frac{1}{h} \|1\|_{L^2(K)} \leq c}. \end{aligned}$$

The final estimate results by deriving a bound for the remaining term (\star) . To improve the readability we skip the index i and get

$$\begin{aligned} (\star) &= \left| \mathbf{P}_h \frac{1}{|E|} \int_E (\tilde{\mathbf{v}} \cdot \mathbf{n}_{E^l}) \mathbf{n}_{E^l} - (\tilde{\mathbf{v}} \cdot \tilde{\mathbf{n}}_{E^l}) \mathbf{n}_E + (\tilde{\mathbf{v}} \cdot \tau_{E^l}) \tau_{E^l} - (\tilde{\mathbf{v}} \cdot \tau_E) \tau_E \right. \\ &\quad \left. + \underbrace{(\tilde{\mathbf{v}} \cdot \mathbf{n}) \mathbf{n}}_{=0} d\sigma_h \right| \\ &= \left| \frac{1}{|E|} \int_E (\tilde{\mathbf{v}} \cdot \mathbf{n}_{E^l}) (\mathbf{P}_h \mathbf{n}_{E^l} - \mathbf{n}_E) + (\tilde{\mathbf{v}} \cdot \tau_{E^l}) (\mathbf{P}_h \tau_{E^l} - \tau_E) d\sigma_h \right| \\ &\leq ch^2 \frac{1}{h} \int_E |\tilde{\mathbf{v}} \cdot \mathbf{n}_{E^l}| + |\tilde{\mathbf{v}} \cdot \tau_{E^l}| d\sigma_h \leq ch \|1 \cdot \tilde{\mathbf{v}}\|_{L^1(E)} \\ &\leq ch^{\frac{3}{2}} \|\tilde{\mathbf{v}}\|_{L^2(E)} \leq ch \|\tilde{\mathbf{v}}\|_{H^1(K)}, \end{aligned}$$

where the Cauchy-Schwarz inequality is applied in the second estimate and the trace inequality is used in the last estimate.

Estimate (35) is proven similarly. It holds that

$$\begin{aligned} \left\| \mathbf{P}(\Pi_h \mathbf{v} - \Pi_h^{tan} \mathbf{v}) \right\|_{L^2(K)} &= \left\| \sum_{i=1}^3 \phi_i \mathbf{P}(\alpha_i(\tilde{\mathbf{v}}) - \alpha_i^{tan}(\tilde{\mathbf{v}})) \right\|_{L^2(K)} \\ &\leq \sum_{i=1}^3 \left(\underbrace{\left| \mathbf{P}_h(\alpha_i(\tilde{\mathbf{v}}) - \alpha_i^{tan}(\tilde{\mathbf{v}})) \right|}_{\leq ch, (*)} + \max_K \underbrace{\| \mathbf{P} - \mathbf{P}_h \|}_{\leq ch, (24)} \underbrace{|\alpha_i(\tilde{\mathbf{v}}) - \alpha_i^{tan}(\tilde{\mathbf{v}})|}_{\leq c \|\tilde{\mathbf{v}}\|_{H^1(K)}} \right) \underbrace{\|\phi_i\|_{L^2(K)}}_{\leq 1 \|1\|_{L^2(K)} \leq ch}. \end{aligned}$$

Estimate (36) is shown by combining (34) and (35). \square

4.1 Energy error estimate

The aim of this section is to derive the energy error in the discrete energy norm. The main tool used in the derivation is Strang's second Lemma.

Theorem 4.4 (Strang's second Lemma). *Let $\mathbf{u} \in H_{tan}^1(\Gamma)$ be the exact solution of (12), $\tilde{\mathbf{u}}$ be its extension to U and $\mathbf{u}_h \in \mathbf{V}_h$ be the discrete solution of (19). Then the following estimates holds*

$$\|\tilde{\mathbf{u}} - \mathbf{u}_h\|_h \leq \underbrace{c \inf_{\mathbf{v}_h \in \mathbf{V}_h} \|\tilde{\mathbf{u}} - \mathbf{v}_h\|_h}_{\text{approximation error}} + \underbrace{\sup_{\mathbf{v}_h \in \mathbf{V}_h} \frac{a_h(\tilde{\mathbf{u}}, \mathbf{v}_h) - (\tilde{\mathbf{f}}, \mathbf{v}_h)}{\|\mathbf{v}_h\|_h}}_{\text{nonconformity error}}. \quad (39)$$

The nonconformity error is bounded in Lemma 4.5.

Lemma 4.5 (Nonconformity Error Estimate). *Let \mathbf{u} be the solution of (12) and $\tilde{\mathbf{u}}$ be its extension to U defined by (4). Then the following error estimate holds*

$$|a_h(\tilde{\mathbf{u}}, \mathbf{v}_h) - (\tilde{\mathbf{f}}, \mathbf{v}_h)_{\Gamma_h}| \leq ch \|\mathbf{u}\|_{H^2(\Gamma)} \|\mathbf{v}_h\|_h, \quad (40)$$

for any $\mathbf{v}_h \in \mathbf{V}_h^{tan}$.

Proof. Let $\mathbf{v}_h^{+,l} := \mathbf{v}_h^l|_{K^+}$. We reformulate the statement (40) to

$$|a_h(\tilde{\mathbf{u}}, \mathbf{v}_h) - (\tilde{\mathbf{f}}, \mathbf{v}_h)_{\Gamma_h}| = |a_h(\tilde{\mathbf{u}}, \mathbf{v}_h) - (\mathbf{f}, \mathbf{v}_h^l)_{\Gamma} + (\mathbf{f}, \mathbf{v}_h^l)_{\Gamma} - (\tilde{\mathbf{f}}, \mathbf{v}_h)_{\Gamma_h}| \quad (41)$$

$$\leq \underbrace{|a_h(\tilde{\mathbf{u}}, \mathbf{v}_h) - a(\mathbf{u}, \mathbf{v}_h^l) + (\mathbf{f}, \mathbf{v}_h^l) - (\tilde{\mathbf{f}}, \mathbf{v}_h)_{\Gamma_h}|}_I \quad (42)$$

$$+ \underbrace{\sum_{E^l} \left| \int_{E^l} \mathbf{v}_h^{+,l} \cdot \nabla_{\Gamma} \mathbf{u}_{E^l}^+ + \mathbf{v}_h^{-,l} \cdot \nabla_{\Gamma} \mathbf{u}_{E^l}^- d\sigma \right|}_{II}, \quad (43)$$

where we used the triangle inequality and Green's formula (23) in the last bound. The terms collected in I are the geometric error, whereas the jump terms that

arise due to nonconformity of the element are collected in II .

Geometric error I . The estimate for I is derived by applying the arguments used in Lemma 5.4 in [12]:

$$I = |a_h(\tilde{\mathbf{u}}, \mathbf{v}_h) - a(\mathbf{u}, \mathbf{v}_h^l) + (\mathbf{f}, \mathbf{v}_h^l) - (\tilde{\mathbf{f}}, \mathbf{v}_h)_{\Gamma_h}| \leq h \|\mathbf{v}_h\|_h \|\mathbf{u}\|_{H^2(\Gamma)}. \quad (44)$$

Jump terms II . We use that $\mathbf{v}_h^l = v_n^l \mathbf{n}_E^l + v_t^l \tau_E^l$ and reformulate II to

$$\begin{aligned} II = \sum_{E^l} \left| \int_{E^l} [\mathbf{v}_h^l] \cdot \nabla_{\Gamma} \mathbf{u}_{E^l}^+ d\sigma \right| &= \underbrace{\sum_{E^l} \left| \int_{E^l} [v_n^l \mathbf{n}_E^l] \cdot \nabla_{\Gamma} \mathbf{u}_{E^l}^+ d\sigma \right|}_{II_1} \\ &+ \underbrace{\sum_{E^l} \left| \int_{E^l} [v_t^l \tau_E^l] \cdot \nabla_{\Gamma} \mathbf{u}_{E^l}^+ d\sigma \right|}_{II_2}. \end{aligned} \quad (45)$$

We outline the derivation of an estimate for II_1 . A bound for II_2 is derived similarly. Note that \mathbf{n}_{E^l} is the outer conormal vector to K^l on Γ , while \mathbf{n}_E^l is the lift of \mathbf{n}_E from Γ_h to Γ . It holds that $\mathbf{n}_{E^l}^+ = -\mathbf{n}_{E^l}^-$, but $\mathbf{n}_E^+ \neq -\mathbf{n}_E^-$. We use the fact that $\mathbf{P}^T = \mathbf{P}$ and $\mathbf{P} \nabla_{\Gamma} \mathbf{u} = \nabla_{\Gamma} \mathbf{u}$. The normal component II_1 is bounded as

$$\begin{aligned} II_1 &= \sum_{E^l} \left| \int_{E^l} \left(\mathbf{P}(v_n^{+,l} \mathbf{n}_E^{+,l}) - \mathbf{P}(v_n^{-,l} \mathbf{n}_E^{-,l}) \right) \cdot \nabla_{\Gamma} \mathbf{u}_{E^l}^+ d\sigma \right| \\ &\leq \sum_{E^l} \left| \int_{E^l} \left(v_n^{+,l} (\mathbf{P} \mathbf{n}_E^{+,l} - \mathbf{n}_{E^l}^+) - v_n^{-,l} (\mathbf{P} \mathbf{n}_E^{-,l} - \mathbf{n}_{E^l}^-) \right) \cdot \nabla_{\Gamma} \mathbf{u}_{E^l}^+ d\sigma \right| \\ &+ \sum_{E^l} \left| \int_{E^l} (v_n^{+,l} \mathbf{n}_{E^l}^+ - v_n^{-,l} \mathbf{n}_{E^l}^-) \cdot \nabla_{\Gamma} \mathbf{u}_{E^l}^+ d\sigma \right| \\ &\leq \sum_{E^l} \underbrace{|\mathbf{P} \mathbf{n}_E^{+,l} - \mathbf{n}_{E^l}^+|_{L^\infty(E^l)}}_{O(h^2), (25)} |v_n^{+,l}|_{L^2(E^l)} |\nabla_{\Gamma} \mathbf{u}| \\ &+ \sum_{E^l} \underbrace{|\mathbf{P} \mathbf{n}_E^{-,l} - \mathbf{n}_{E^l}^-|_{L^\infty(E^l)}}_{O(h^2), (25)} |v_n^{-,l}|_{L^2(E^l)} |\nabla_{\Gamma} \mathbf{u}| + \sum_{E^l} \underbrace{\left| \int_{E^l} [v_n^l] \mathbf{n}_{E^l}^+ \cdot \nabla_{\Gamma} \mathbf{u}_{E^l}^+ d\sigma \right|}_{II_\star}. \end{aligned} \quad (46)$$

We introduce the mean value of the scalar normal component v_n^l along the corresponding edge E^l as \bar{v}_n^l and use the fact that $[\bar{v}_n^l] = 0$. Thus, II_\star is reformulated to

$$II_\star = \left| \int_{E^l} [v_n^l - \bar{v}_n^l] \mathbf{n}_{E^l}^+ \cdot (\nabla_{\Gamma} \mathbf{u}) \mathbf{n}_{E^l}^+ d\sigma \right|.$$

In the next step, we include the covariant derivative on Γ_h to II_\star and use the fact that $\nabla_{\Gamma_h} \Pi_h^{tan} \mathbf{u}$ is piecewise constant per cell.

$$\begin{aligned}
II_\star &= \left| \int_{E^l} [v_n^l - \bar{v}_n^l] \mathbf{n}_{E^l}^+ \cdot \left(\nabla_\Gamma \mathbf{u} - (\nabla_{\Gamma_h} \tilde{\mathbf{u}})^l \right) \mathbf{n}_{E^l}^+ d\sigma \right| \\
&\quad + \left| \int_{E^l} [v_n^l - \bar{v}_n^l] \mathbf{n}_{E^l}^+ \cdot (\nabla_{\Gamma_h} (\tilde{\mathbf{u}} - \Pi_h^{tan} \mathbf{u}))^l \mathbf{n}_{E^l}^+ d\sigma \right| \\
&\leq \left(\int_{E^l} |[v_n^l - \bar{v}_n^l]|^2 d\sigma \right)^{\frac{1}{2}} \left(\int_{E^l} |\nabla_\Gamma \mathbf{u} - (\nabla_{\Gamma_h} \tilde{\mathbf{u}})^l|^2 d\sigma \right)^{\frac{1}{2}} \\
&\quad + \left(\int_{E^l} |[v_n^l - \bar{v}_n^l]|^2 d\sigma \right)^{\frac{1}{2}} \left(\int_{E^l} |\nabla_{\Gamma_h} (\tilde{\mathbf{u}} - \Pi_h^{tan} \mathbf{u}))^l|^2 d\sigma \right)^{\frac{1}{2}},
\end{aligned}$$

where we used the Cauchy-Schwarz inequality in the last step. The term II_\star is bounded by the application of the estimates (47)-(49) listed below: Estimate (47) is achieved by applying the trace inequality and Poincaré's inequality for the discrete function $v_n^l - \bar{v}_n^l$, which is zero in the edge midpoint. Thus, we get

$$\int_{E^l} |[v_n^l - \bar{v}_n^l]|^2 d\sigma \leq ch \left(|v_h^l|_{H^1(K^l, +)}^2 + |v_h^l|_{H^1(K^l, -)}^2 \right). \quad (47)$$

We use the trace inequality and the interpolation estimate (34) and get

$$\int_{E^l} |\nabla_{\Gamma_h} (\tilde{\mathbf{u}} - \Pi_h^{tan} \mathbf{u}))^l|^2 d\sigma \leq ch |\mathbf{u}|_{H^2(K^l)}^2. \quad (48)$$

The estimate

$$\int_{E^l} |\nabla_\Gamma \mathbf{u} - (\nabla_{\Gamma_h} \tilde{\mathbf{u}})^l|^2 d\sigma \leq ch |\mathbf{u}|_{H^1(K)}^2, \quad (49)$$

results by using arguments provided in Lemma 5.4 [12]. By the combination of I and II the final estimate results. \square

Theorem 4.6 (Energy Error Estimate). *Let $\tilde{\mathbf{u}}$ be the extension of the exact solution of (12) to U and \mathbf{u}_h the discrete solution of (19). Then the following error estimate holds*

$$\|\tilde{\mathbf{u}} - \mathbf{u}_h\|_h \leq ch \|\mathbf{f}\|_{L^2(\Gamma)}. \quad (50)$$

Proof. Lemma 4.5 as well as the regularity estimate (13) give

$$\sup_{\mathbf{v}_h \in \mathbf{V}_h} \frac{|a_h(\tilde{\mathbf{u}}, \mathbf{v}_h) - (\mathbf{f}, \mathbf{v}_h^l)|}{\|\mathbf{v}_h\|_h} \leq ch \|\mathbf{f}\|_{L^2(\Gamma)}. \quad (51)$$

Next, we consider the approximation error:

$$\inf_{\mathbf{v}_h \in \mathbf{V}_h} \|\tilde{\mathbf{u}} - \mathbf{v}_h\|_h \leq \|\tilde{\mathbf{u}} - \Pi_h^{tan} \mathbf{u}\|_h \leq ch \|\tilde{\mathbf{u}}\|_{H^2(\Gamma_h)} \leq ch \|\mathbf{f}\|_{L^2(\Gamma)}, \quad (52)$$

where we used (36) in the second bound and the regularity estimate (13) in the last inequality. The proof is completed by the combination of Strang's second Lemma (4.4) with the error bounds (51) and (52). \square

4.2 L^2 -error estimate

The derivation of the L^2 -error estimate is based on the Aubin-Nitsche trick. The dual problem reads as

$$\begin{aligned} \text{Find } \mathbf{z} \in H_{tan}^1(\Gamma) \text{ s.t. } \quad & a(\mathbf{v}, \mathbf{z}) = (\mathbf{v}, \mathbf{g}), \quad \forall \mathbf{v} \in H_{tan}^1(\Gamma) \\ & \mathbf{g} = \mathbf{P}(\mathbf{u} - \mathbf{u}_h^l) \in L^2(\Gamma). \end{aligned} \quad (53)$$

The following regularity estimate holds true (cf. [12, eq. (5.158)]).

$$\|\mathbf{v}\|_{H^2(\Gamma)} \leq c\|\mathbf{g}\|_{L^2(\Gamma)}. \quad (54)$$

The corresponding discrete dual problem reads as

$$\text{find } \mathbf{z}_h \in \mathbf{V}_h \text{ s.t. } \quad a_h(\mathbf{v}_h, \mathbf{z}_h) = (\mathbf{v}_h, \tilde{\mathbf{g}})_{\Gamma_h}, \quad \forall \mathbf{v}_h \in \mathbf{V}_h. \quad (55)$$

Based on Theorem 4.6 the following energy estimate results for the dual solution

$$\|\tilde{\mathbf{z}} - \mathbf{z}_h\|_h \leq ch\|\mathbf{g}\|_{L^2(\Gamma)}. \quad (56)$$

Lemma 4.7 (Primal and dual interpolation estimate). *Let \mathbf{u} be the solution of the primal problem (12) and $\mathbf{z} \in H^2(\Gamma)$ be a vector field. It holds that*

$$a_h(\tilde{\mathbf{u}}, \tilde{\mathbf{z}} - \mathbf{P}\Pi_h^{tan}\mathbf{z}) \leq ch^2\|\mathbf{u}\|_{H^2(\Gamma)}\|\mathbf{z}\|_{H^2(\Gamma)}. \quad (57)$$

Analog, the following estimate holds for a vector field $\mathbf{u} \in H^2(\Gamma)$ and the dual solution \mathbf{z} of (54)

$$a_h(\tilde{\mathbf{u}} - \mathbf{P}\Pi_h^{tan}\mathbf{u}, \tilde{\mathbf{z}}) \leq ch^2\|\mathbf{u}\|_{H^2(\Gamma)}\|\mathbf{z}\|_{H^2(\Gamma)}. \quad (58)$$

Proof. We note that $\Delta_{\Gamma_h}(\Pi_h^{tan}\mathbf{u}) = 0$. We apply Green's formula (23) and get

$$\begin{aligned} a_h(\tilde{\mathbf{u}}, \tilde{\mathbf{z}} - \mathbf{P}\Pi_h^{tan}\mathbf{z}) &= a_h(\Pi_h^{tan}\mathbf{u}, \tilde{\mathbf{z}} - \mathbf{P}\Pi_h^{tan}\mathbf{z}) + a_h(\tilde{\mathbf{u}} - \Pi_h^{tan}\mathbf{u}, \tilde{\mathbf{z}} - \mathbf{P}\Pi_h^{tan}\mathbf{z}) \\ &= \sum_K \left(\Pi_h^{tan}\mathbf{u} - \underbrace{(\Delta_{\Gamma_h}(\Pi_h^{tan}\mathbf{u}))}_{=0}, \tilde{\mathbf{z}} - \mathbf{P}\Pi_h^{tan}\mathbf{z} \right)_K \\ &\quad + \sum_E \underbrace{\left(\nabla_{\Gamma_h}^+(\Pi_h^{tan}\mathbf{u})\mathbf{n}_E^+ + \nabla_{\Gamma_h}^-(\Pi_h^{tan}\mathbf{u})\mathbf{n}_E^-, \tilde{\mathbf{z}} - \mathbf{P}\Pi_h^{tan}\mathbf{z} \right)}_{I_\star}_E \\ &\quad + \sum_K \left(\tilde{\mathbf{u}} - \Pi_h^{tan}\mathbf{u} - (\Delta_{\Gamma_h}(\tilde{\mathbf{u}} - \Pi_h^{tan}\mathbf{u})), \tilde{\mathbf{z}} - \mathbf{P}\Pi_h^{tan}\mathbf{z} \right)_K \\ &\quad + \sum_E \underbrace{\left(\nabla_{\Gamma_h}^+(\tilde{\mathbf{u}} - \Pi_h^{tan}\mathbf{u})\mathbf{n}_E^+ + \nabla_{\Gamma_h}^-(\tilde{\mathbf{u}} - \Pi_h^{tan}\mathbf{u})\mathbf{n}_E^-, \tilde{\mathbf{z}} - \mathbf{P}\Pi_h^{tan}\mathbf{z} \right)}_{I_1}_E \\ &\leq \sum_K \left(\int_K |\Delta_{\Gamma_h}\tilde{\mathbf{u}}|^2 d\sigma_h \right)^{\frac{1}{2}} \left(\int_K |\mathbf{P}(\tilde{\mathbf{z}} - \Pi_h^{tan}\mathbf{z})|^2 d\sigma_h \right)^{\frac{1}{2}} \\ &\quad + \sum_K \left(\int_K |\tilde{\mathbf{u}}|^2 d\sigma_h \right)^{\frac{1}{2}} \left(\int_K |\mathbf{P}(\tilde{\mathbf{z}} - \Pi_h^{tan}\mathbf{z})|^2 d\sigma_h \right)^{\frac{1}{2}} + I_1 + I_\star \\ &\leq ch^2 \sum_{K^l} \left(\|\mathbf{u}\|_{H^2(K^l)}\|\mathbf{z}\|_{H^2(K^l)} + \|\mathbf{u}\|_{H^2(K^l)}\|\mathbf{z}\|_{H^2(K^l)} \right) + I_1 + I_\star, \end{aligned}$$

where we use the Cauchy-Schwarz inequality in the first inequality and estimate (35) as well as the norm equivalences given in Lemma 4.2 in the second estimate. **Term I_1 .** To derive an estimate for I_1 we use the Cauchy-Schwarz inequality and get

$$\begin{aligned} I_1 &\leq I_2^{\frac{1}{2}} I_3^{\frac{1}{2}}, \\ I_2 &= \int_E |\nabla_{\Gamma_h}^+ (\tilde{\mathbf{u}} - \Pi_h^{tan} \mathbf{u}) \mathbf{n}_E^+ + \nabla_{\Gamma_h}^- (\tilde{\mathbf{u}} - \Pi_h^{tan} \mathbf{u}) \mathbf{n}_E^-|^2 d\sigma_h, \\ I_3 &= \int_E |\tilde{\mathbf{z}} - \mathbf{P} \Pi_h^{tan} \mathbf{z}|^2 d\sigma_h. \end{aligned}$$

Based on the trace inequality and the interpolation estimates (34) and (35) we bound I_2 and I_3 as

$$\begin{aligned} I_2 &= \int_E |\nabla_{\Gamma_h}^+ (\tilde{\mathbf{u}} - \Pi_h^{tan} \mathbf{u}) \mathbf{n}_E^+ + \nabla_{\Gamma_h}^- (\tilde{\mathbf{u}} - \Pi_h^{tan} \mathbf{u}) \mathbf{n}_E^-|^2 d\sigma_h \\ &\leq h |\tilde{\mathbf{u}}|_{H^2(K^-)}^2 + h |\tilde{\mathbf{u}}|_{H^2(K^+)}^2, \end{aligned} \quad (59)$$

and

$$I_3 = \int_E |\mathbf{P}(\tilde{\mathbf{z}} - \Pi_h^{tan} \mathbf{z})|^2 d\sigma_h \leq ch^3 |\tilde{\mathbf{z}}|_{H^2(K)}^2. \quad (60)$$

This gives us

$$|I_1| \leq c \left(h |\tilde{\mathbf{u}}|_{H^2(K)}^2 \right)^{\frac{1}{2}} \left(h^3 |\tilde{\mathbf{z}}|_{H^2(K)}^2 \right)^{\frac{1}{2}} \leq ch^2 \|\mathbf{u}\|_{H^2(K^l)} \|\mathbf{z}\|_{H^2(K^l)},$$

where we apply (28) in the last step.

Term I_\star To derive a bound for I_\star we apply the Cauchy-Schwarz inequality and get

$$I_\star = \underbrace{\left(\int_E |\nabla_{\Gamma_h}^+ (\Pi_h^{tan} \mathbf{u}) \mathbf{n}_E^+ + \nabla_{\Gamma_h}^- (\Pi_h^{tan} \mathbf{u}) \mathbf{n}_E^-|^2 d\sigma_h \right)^{\frac{1}{2}}}_{I_{\star\star}} \underbrace{\left(\int_E |\tilde{\mathbf{z}} - \mathbf{P} \Pi_h^{tan} \mathbf{z}|^2 d\sigma_h \right)^{\frac{1}{2}}}_{\leq ch^{\frac{3}{2}} \|\tilde{\mathbf{z}}\|_{H^2(K)}, (60)}.$$

To bound $I_{\star\star}$ we introduce the covariant derivative on Γ , use the fact that $\mathbf{n}_{E^l}^+ = -\mathbf{n}_{E^l}^-$ and apply the triangle inequality.

$$\begin{aligned} I_{\star\star} &\leq |(\nabla_{\Gamma_h}^+ \Pi_h^{tan} \mathbf{u} - \nabla_{\Gamma}(\widetilde{\Pi_h^{tan} \mathbf{u}})^l)|_{L^2(E)} |\mathbf{n}_E^+|_{L^2(E)} \\ &\quad + |(\nabla_{\Gamma_h}^- \Pi_h^{tan} \mathbf{u} - \nabla_{\Gamma}(\widetilde{\Pi_h^{tan} \mathbf{u}})^l)|_{L^2(E)} |\mathbf{n}_E^-|_{L^2(E)} \\ &\quad + |\nabla_{\Gamma}(\widetilde{\Pi_h^{tan} \mathbf{u}})^l|_{L^2(E)} \left(\underbrace{|\mathbf{P}(\mathbf{n}_E^+ - \mathbf{n}_{E^l}^+)|_{L^\infty(E)}}_{\leq ch^2 (25)} + \underbrace{|\mathbf{P} \mathbf{n}_E^- - \mathbf{n}_{E^l}^-|_{L^\infty(E)}}_{\leq ch^2 (25)} \right) \\ &\leq ch^{\frac{1}{2}} \|\tilde{\mathbf{u}}\|_{H^1(K)} + ch^{\frac{3}{2}} \|\tilde{\mathbf{u}}\|_{H^1(K)}, \end{aligned}$$

where we used the same arguments as in Lemma 5.3 of [12] to bound the difference in the operators. By using the norm equivalence (28) we get

$$I_\star \leq ch^{\frac{1}{2}} \|\tilde{\mathbf{u}}\|_{H^2(K)} h^{\frac{3}{2}} \|\tilde{\mathbf{z}}\|_{H^2(K)} \leq h^2 \|\mathbf{u}\|_{H^2(K')} \|\mathbf{z}\|_{H^2(K')}.$$

Finally, we obtain the desired estimate

$$a_h(\tilde{\mathbf{u}}, \tilde{\mathbf{z}} - \mathbf{P}\Pi_h^{tan}\mathbf{z}) \leq ch^2 \|\mathbf{u}\|_{H^2(\Gamma)} \|\mathbf{z}\|_{H^2(\Gamma)}.$$

□

Based on the lemma above we prove the following estimate for the consistency error.

Lemma 4.8 (Primal and dual consistency error estimate). *Let \mathbf{u} be the solution to the primal problem (12) and \mathbf{z} be the solution to the dual problem (53). \mathbf{u}_h is the discrete solution of (19) and \mathbf{z}_h the discrete solution of (55). Then the following estimates hold*

$$\begin{aligned} a_h(\tilde{\mathbf{u}}, \tilde{\mathbf{z}} - \mathbf{z}_h) - \left((\mathbf{f}, \mathbf{z})_\Gamma - (\tilde{\mathbf{f}}, \mathbf{z}_h)_{\Gamma_h} \right) &\leq ch^2 \|\mathbf{f}\|_{L^2(\Gamma)} \|\mathbf{g}\|_{L^2(\Gamma)}, \\ a_h(\tilde{\mathbf{u}} - \mathbf{u}_h, \tilde{\mathbf{z}}) - \left((\mathbf{u}, \mathbf{g})_\Gamma - (\mathbf{u}_h, \tilde{\mathbf{g}})_{\Gamma_h} \right) &\leq ch^2 \|\mathbf{f}\|_{L^2(\Gamma)} \|\mathbf{g}\|_{L^2(\Gamma)}. \end{aligned}$$

Proof. The first and second inequality can be proven analogously. We outline the proof of the first inequality below and use that $\tilde{\mathbf{f}} = \mathbf{P}\tilde{\mathbf{f}}$.

$$\begin{aligned} &a_h(\tilde{\mathbf{u}}, \tilde{\mathbf{z}} - \mathbf{z}_h \pm \mathbf{P}\Pi_h^{tan}\mathbf{z}) - (\mathbf{f}, \mathbf{z})_\Gamma + (\tilde{\mathbf{f}}, \mathbf{z}_h \pm \Pi_h^{tan}\mathbf{z} \pm \tilde{\mathbf{z}})_{\Gamma_h} \\ &= \underbrace{a_h(\tilde{\mathbf{u}}, \tilde{\mathbf{z}} - \mathbf{P}\Pi_h^{tan}\mathbf{z})}_{I_1} + \underbrace{(\tilde{\mathbf{f}}, \tilde{\mathbf{z}})_{\Gamma_h} - (\mathbf{f}, \mathbf{z})_\Gamma}_{I_2} + \underbrace{(\tilde{\mathbf{f}}, -\tilde{\mathbf{z}} + \Pi_h^{tan}\mathbf{z})_{\Gamma_h}}_{I_3} \\ &\quad + \underbrace{a_h(\tilde{\mathbf{u}}, \mathbf{P}\Pi_h^{tan}\mathbf{z} - \mathbf{z}_h) + (\tilde{\mathbf{f}}, \mathbf{z}_h - \Pi_h^{tan}\mathbf{z})_{\Gamma_h}}_{I_4}. \end{aligned}$$

According to Lemma 4.7 I_1 is reformulated to

$$|I_1| = a_h(\tilde{\mathbf{u}}, \tilde{\mathbf{z}} - \mathbf{P}\Pi_h^{tan}\mathbf{z}) \leq ch^2 \|\mathbf{u}\|_{H^2(\Gamma)} \|\mathbf{z}\|_{H^2(\Gamma)}.$$

Following the arguments given in Lemma 5.4 in [12] and using the regularity estimate (13) one gets

$$|I_2| = |(\tilde{\mathbf{f}}, \tilde{\mathbf{z}})_{\Gamma_h} - (\mathbf{f}, \mathbf{z})_\Gamma| \leq ch^2 \|\mathbf{f}\|_{L^2(\Gamma)} \|\mathbf{z}\|_{L^2(\Gamma)}.$$

The combination of the Cauchy-Schwarz inequality, the interpolation estimate (35), the regularity estimate (54) and the fact that $\tilde{\mathbf{f}} = \mathbf{P}\tilde{\mathbf{f}}$ and $\mathbf{P}^T = \mathbf{P}$ gives

$$\begin{aligned} |I_3| &= \left(\mathbf{P}\tilde{\mathbf{f}}, \Pi_h^{tan}\mathbf{z} - \tilde{\mathbf{z}} \right)_{\Gamma_h} \leq \left(\int_{\Gamma_h} \tilde{\mathbf{f}}^2 d\sigma_h \right)^{\frac{1}{2}} \left(\int_{\Gamma_h} |\mathbf{P}(\Pi_h^{tan}\mathbf{z} - \tilde{\mathbf{z}})|^2 d\sigma_h \right)^{\frac{1}{2}} \\ &\leq ch^2 \|\tilde{\mathbf{f}}\|_{L^2(\Gamma)} \|\tilde{\mathbf{z}}\|_{H^2(\Gamma_h)}. \end{aligned}$$

We bound I_4 as follows

$$\begin{aligned}
I_4 &= a_h(\tilde{\mathbf{u}}, \mathbf{P}\Pi_h^{tan}\mathbf{z} - \mathbf{z}_h) + (\tilde{\mathbf{f}}, \mathbf{z}_h - \Pi_h^{tan}\mathbf{z})_{\Gamma_h} \\
&\leq ch\|\mathbf{u}\|_{H^2(\Gamma)}\|\mathbf{P}\Pi_h^{tan}\mathbf{z} \pm \tilde{\mathbf{z}} - \mathbf{z}_h\|_h \\
&\leq ch\|\mathbf{u}\|_{H^2(\Gamma)}\left(\|\mathbf{P}\|_h\|\Pi_h^{tan}\mathbf{z} - \tilde{\mathbf{z}}\|_h + \|\tilde{\mathbf{z}} - \mathbf{z}_h\|_h\right) \\
&\leq ch\|\mathbf{u}\|_{H^2(\Gamma_h)}\left(ch\|\mathbf{z}\|_{H^2(\Gamma_h)} + h\|\mathbf{g}\|_{L^2(\Gamma_h)}\right),
\end{aligned}$$

where we apply the same argumentation as in Lemma 4.5 in the first estimate, the energy estimate (56), interpolation estimate (35) as well as the norm equivalence provided in Lemma 4.2 in the third bound. The final estimate results by applying the regularity estimates (13) and (54) to the bounds derived for I_1 to I_4 . \square

Theorem 4.9 (L^2 Error Estimate). *Let \mathbf{u} be the primal solution to (12), $\tilde{\mathbf{u}}$ be the extension to a neighborhood and \mathbf{u}_h is the discrete solution of (19). Then the following error estimate holds*

$$\|\mathbf{P}(\tilde{\mathbf{u}} - \mathbf{u}_h)\|_{L^2(\Gamma_h)} \leq ch^2\|\mathbf{f}\|_{L^2(\Gamma)}.$$

Proof. Note that $\mathbf{P}\tilde{\mathbf{u}} = \tilde{\mathbf{u}}$ and $\mathbf{P}\tilde{\mathbf{g}} = \tilde{\mathbf{g}}$. First, we introduce the geometrical error, terms I_1, I_2 , by adding and subtracting suitable terms.

$$\begin{aligned}
\|\mathbf{P}(\tilde{\mathbf{u}} - \mathbf{u}_h)\|_{L^2(\Gamma_h)}^2 &= (\tilde{\mathbf{u}} - \mathbf{u}_h, \mathbf{P}\tilde{\mathbf{g}})_{\Gamma_h} \\
&= \underbrace{(\tilde{\mathbf{u}}, \tilde{\mathbf{g}})_{\Gamma_h} - (\mathbf{u}, \mathbf{g})_{\Gamma}}_{I_1} - (\mathbf{u}_h, \tilde{\mathbf{g}})_{\Gamma_h} - \underbrace{a(\mathbf{u}, \mathbf{z}) + a_h(\tilde{\mathbf{u}}, \tilde{\mathbf{z}})}_{I_2} \\
&\quad - a_h(\tilde{\mathbf{u}}, \tilde{\mathbf{z}}) + a(\mathbf{u}, \mathbf{z}).
\end{aligned}$$

In second step, we add and subtract further terms to apply the primal and dual energy error estimate to term I_3

$$\begin{aligned}
\|\mathbf{P}(\tilde{\mathbf{u}} - \mathbf{u}_h)\|_{L^2(\Gamma_h)}^2 &= I_1 + I_2 + (\mathbf{u}, \mathbf{g})_{\Gamma} - (\mathbf{u}_h, \tilde{\mathbf{g}})_{\Gamma_h} - a_h(\tilde{\mathbf{u}}, \tilde{\mathbf{z}}) + a(\mathbf{u}, \mathbf{z}) \\
&\quad + \underbrace{a_h(\tilde{\mathbf{u}} - \mathbf{u}_h, \tilde{\mathbf{z}} - \mathbf{z}_h)}_{I_3} - a_h(\tilde{\mathbf{u}}, \tilde{\mathbf{z}}) + a_h(\mathbf{u}_h, \tilde{\mathbf{z}}) \\
&\quad + a_h(\tilde{\mathbf{u}}, \mathbf{z}_h) - a_h(\mathbf{u}_h, \mathbf{z}_h).
\end{aligned}$$

We make use of the relation of (12) and (20) and reorder the terms to insert the primal and dual consistency error, I_4 and I_5 .

$$\begin{aligned}
&= I_1 + I_2 + I_3 + (\mathbf{u}, \mathbf{g})_{\Gamma} - (\mathbf{u}_h, \tilde{\mathbf{g}})_{\Gamma_h} - a_h(\tilde{\mathbf{u}}, \tilde{\mathbf{z}}) + (\mathbf{f}, \mathbf{z})_{\Gamma} \\
&\quad - a_h(\tilde{\mathbf{u}}, \tilde{\mathbf{z}}) + a_h(\mathbf{u}_h, \tilde{\mathbf{z}}) + a_h(\tilde{\mathbf{u}}, \mathbf{z}_h) - (\tilde{\mathbf{f}}, \mathbf{z}_h)_{\Gamma_h} \\
&= I_1 + I_2 + I_3 - \underbrace{a_h(\tilde{\mathbf{u}} - \mathbf{u}_h, \tilde{\mathbf{z}}) + (\mathbf{u}, \mathbf{g})_{\Gamma} - (\mathbf{u}_h, \tilde{\mathbf{g}})_{\Gamma_h}}_{I_5} \\
&\quad - \underbrace{a_h(\tilde{\mathbf{u}}, \tilde{\mathbf{z}} - \mathbf{z}_h) + (\mathbf{f}, \mathbf{z})_{\Gamma} - (\tilde{\mathbf{f}}, \mathbf{z}_h)_{\Gamma_h}}_{I_4}.
\end{aligned}$$

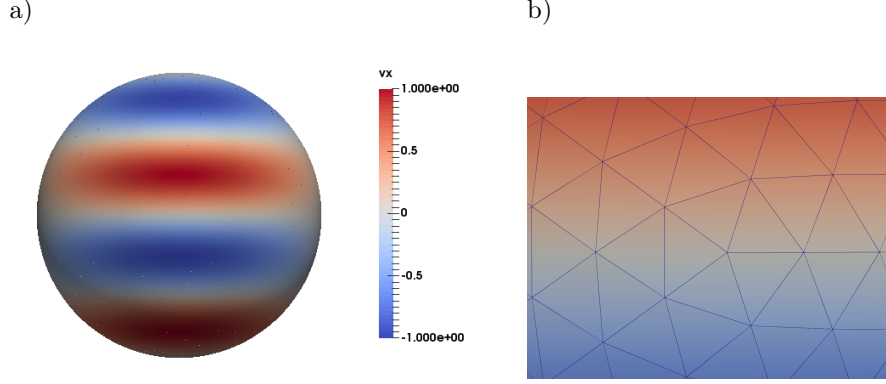


Figure 2: *Left:* Refined icosahedral mesh projected onto the surface of the sphere with a side length of 158 km. *Right:* First component of the velocity. Numerical solution to equation (63)

Using the same arguments as in Lemma 5.4 of [12] and applying the regularity estimates (13) and (54) as well as the norm equivalences provided in Lemma 4.2 one gets

$$|I_1| \leq ch^2 \|\tilde{\mathbf{u}}\|_{L^2(\Gamma_h)} \|\tilde{\mathbf{g}}\|_{L^2(\Gamma_h)} \leq ch^2 \|\mathbf{f}\|_{L^2(\Gamma)} \|\mathbf{g}\|_{L^2(\Gamma)}, \quad (61)$$

$$|I_2| \leq ch^2 \|\mathbf{u}\|_{H^2(\Gamma)} \|\mathbf{z}\|_{H^2(\Gamma)} \leq ch^2 \|\mathbf{f}\|_{L^2(\Gamma)} \|\mathbf{g}\|_{L^2(\Gamma)}. \quad (62)$$

We apply Lemma 4.8 to I_4 and I_5 and get

$$|I_4| + |I_5| \leq ch^2 \|\mathbf{f}\|_{L^2(\Gamma)} \|\mathbf{g}\|_{L^2(\Gamma)}.$$

Finally, we bound I_3 as follows

$$|I_3| \leq c \|\tilde{\mathbf{u}} - \mathbf{u}_h\|_h \|\tilde{\mathbf{z}} - \mathbf{z}_h\|_h \leq ch^2 \|\mathbf{f}\|_{L^2(\Gamma)} \|\mathbf{g}\|_{L^2(\Gamma)},$$

where we apply the primal (4.6) and dual energy estimate (56) in the last step. The combination of the bounds for the terms I_1 to I_5 gives the final estimate. \square

5 Numerical results

The setup is realized in the framework of the climate model ICON [19]. In the climate model the Earth is approximated by a sphere with a radius of $R = 6.371229 \cdot 10^6$ m. We use this setup to evaluate the performance of the presented surface Crouzeix-Raviart element. ICON is based on an unstructured triangular mesh. The triangulation is created by a refinement of an icosahedron. Due to the edges of the icosahedron the mesh is not symmetric. A sketch is shown in the right panel of Figure 2. The final grid is created by a projection of the icosahedral faces onto the surface of the sphere. The coordinates of the Cartesian system are labeled as x, y, z . We consider the following problem

$$-\operatorname{div}_\Gamma \left(\frac{\zeta}{2} \nabla_\Gamma \mathbf{v} \right) + \frac{1}{100} \mathbf{v} = \mathbf{f}, \quad (63)$$

where viscosity and right hand side are

$$\zeta = 2.75 \cdot 10^{13}, \quad \mathbf{f} = -\operatorname{div}_\Gamma \left(\frac{\zeta}{2} \nabla_\Gamma \mathbf{v}^* \right) + \frac{1}{100} \mathbf{v}^*, \quad \mathbf{v}^* = \left(\sin(10^{-6} Ry), 0, 0 \right).$$

The analytic solution is given by \mathbf{v}^* . The sphere is approximated by triangular elements with a side length of 316 km, 158 km and 79 km. The error between the exact and the approximate solution is evaluated in the H^1 -norm. According to Theorem 4.9 we consider $\mathbf{P}(\mathbf{u} - \mathbf{u}_h)$ in the L^2 -norm. We present the numerical results in Table 1. In line with Theorem 4.9 and Theorem 4.6 the L2-error converges with quadratic order, $O(h^2)$, and the H^1 -norm converges with first order, $O(h)$.

Table 1: Evaluation of equation (63) discretized with the Crouzeix-Raviart element on refined meshes.

Edge length	Dof	L^2 -error	Order	H^1 -error	Order
316 km	15360	$1.6880 \cdot 10^{-2}$	-	$3.7166 \cdot 10^{-1}$	-
158 km	61440	$4.2288 \cdot 10^{-3}$	2.00	$1.8613 \cdot 10^{-1}$	1.00
79 km	245760	$1.0605 \cdot 10^{-3}$	2.00	$9.3103 \cdot 10^{-2}$	1.00

References

- [1] J. W. BARRETT, H. GARCKE, AND R. NÜRNBERG, *A stable numerical method for the dynamics of fluidic membranes*, Numerische Mathematik, 134 (2016), pp. 783–822, <https://doi.org/10.1007/s00211-015-0787-5>.
- [2] A. BONITO, A. DEMLOW, AND M. LICHT, *A Divergence-Conforming Finite Element Method for the Surface Stokes Equation*, SIAM Journal on Numerical Analysis, 58 (2020), pp. 2764–2798, <https://doi.org/10.1137/19M1284592>.
- [3] A. BONITO, A. DEMLOW, AND R. H. NOCHETTO, *Chapter 1 - Finite element methods for the Laplace–Beltrami operator*, in Geometric Partial Differential Equations - Part I, A. Bonito and R. H. Nochetto, eds., vol. 21 of Handbook of Numerical Analysis, Elsevier, 2020, pp. 1–103, <https://doi.org/10.1016/bs.hna.2019.06.002>.
- [4] P. BRANDNER, T. JANKUHN, S. PRAETORIUS, A. REUSKEN, AND A. VOIGT, *Finite Element Discretization Methods for Velocity-Pressure*

- and Stream Function Formulations of Surface Stokes Equations, SIAM Journal on Scientific Computing, 44 (2022), pp. A1807–A1832, <https://doi.org/10.1137/21M1403126>.
- [5] P. BRANDNER AND A. REUSKEN, *Finite element error analysis of surface Stokes equations in stream function formulation*, ESAIM M2AN, 54 (2020), pp. 2069–2097, <https://doi.org/10.1051/m2an/2020044>.
 - [6] R. COMBLEN, S. LEGRAND, E. DELEERSNIJDER, AND V. LEGAT, *A finite element method for solving the shallow water equations on the sphere*, Ocean Modelling, 28 (2009), pp. 12–23, <https://doi.org/10.1016/j.ocemod.2008.05.004>.
 - [7] M. CROUZEIX AND P.-A. RAVIART, *Conforming and nonconforming finite element methods for solving the stationary Stokes equations. I*, Rev. Franc. Automat. Inform. Rech. Operat., R, 7 (1974), pp. 33–76.
 - [8] A. DEMLOW AND M. NEILAN, *A tangential and penalty-free finite element method for the surface Stokes problem*, 2023, <https://arxiv.org/abs/2307.01435>.
 - [9] G. DZIUK AND C. M. ELLIOTT, *Finite element methods for surface PDEs*, Acta Numerica, 22 (2013), p. 289–396, <https://doi.org/10.1017/S0962492913000056>.
 - [10] S. GROSS, T. JANKUHN, M. A. OLSHANSKII, AND A. REUSKEN, *A Trace Finite Element Method for Vector-Laplacians on Surfaces*, SIAM Journal on Numerical Analysis, 56 (2018), pp. 2406–2429, <https://doi.org/10.1137/17M1146038>.
 - [11] H. GUO, *Surface Crouzeix–Raviart element for the Laplace–Beltrami equation*, Numer. Math., 144 (2020), pp. 527–551.
 - [12] P. HANSBO, M. LARSON, AND K. LARSSON, *Analysis of finite element methods for vector Laplacians on surfaces*, IMA Journal of Numerical Analysis, 40 (2019), pp. 1652–1701, <https://doi.org/10.1093/imanum/drz018>.
 - [13] P. HANSBO AND M. G. LARSON, *A stabilized finite element method for the Darcy problem on surfaces*, IMA Journal of Numerical Analysis, 37 (2016), pp. 1274–1299, <https://doi.org/10.1093/imanum/drw041>.
 - [14] H. HARDERING AND P. PRAETORIUS, *A Parametric Finite-Element Discretization of the Surface Stokes Equations*, 2023, <https://arxiv.org/abs/2309.00931>.
 - [15] H. HARDERING AND S. PRAETORIUS, *Tangential errors of tensor surface finite elements*, IMA Journal of Numerical Analysis, 43 (2022), pp. 1543–1585, <https://doi.org/10.1093/imanum/drac015>.

- [16] M. HOLST AND A. STERN, *Geometric variational crimes: Hilbert complexes, finite element exterior calculus, and problems on hypersurfaces*, Foundations of Computational Mathematics, 12 (2012), pp. 263–293, <https://doi.org/10.1007/s10208-012-9119-7>.
- [17] J. JANKUHN, M. A. OLSHANSKII, A. REUSKEN, AND A. ZHILIAKOV, *Error analysis of higher order Trace Finite Element Methods for the surface Stokes equation*, Journal of Numerical Mathematics, 29 (2021), pp. 245–267, <https://doi.org/10.1515/jnma-2020-0017>.
- [18] T. JANKUHN AND A. REUSKEN, *Trace finite element methods for surface vector-Laplace equations*, IMA Journal of Numerical Analysis, 41 (2020), pp. 48–83, <https://doi.org/10.1093/imanum/drz062>.
- [19] J. JUNGCLAUS, S. J. LORENZ, H. SCHMIDT, V. BROVKIN, N. BRÜGGEMANN, F. CHEGINI, V. GAYLER, M. GIORGETTA, O. GUTJAHR, H. HAAK, S. HAGEMANN, M. HANKE, T. ILYINA, P. KORN, J. KRÖGER, L. LINARDAKIS, C. MEHLMANN, U. MIKOLAJEWICZ, W. MÜLLER, D. NOTZ, H. POHLMANN, D. PUTRASAHAN, T. RADDATZ, L. RAMME, R. REDLER, C. REICK, T. RIDDICK, T. SAM, R. SCHNECK, R. SCHNUR, M. SCHUPFNER, J.-S. VON STORCH, F. WACHSMANN, K.-H. WIENERS, B. STEVENS, J. MAROTZKE, AND M. CLAUSSEN, *The ICON Earth System Model Version 1.0*, Journal of Advances in Modelling Earth Systems, (2021), <https://doi.org/https://doi.org/10.1029/2021MS002813>.
- [20] K. LARSSON AND M. LARSON, *A continuous/discontinuous Galerkin method and a priori error estimates for the biharmonic problem on surfaces*, Math. Comput., 86 (2013), pp. 2613–2649.
- [21] P. LEDERER, L. C., AND J. SCHÖBERL, *Divergence-free tangential finite element methods for incompressible flows on surfaces*, International Journal for Numerical Methods in Engineering, 121 (2019), pp. 2503 – 2533, <https://api.semanticscholar.org/CorpusID:202572792>.
- [22] C. MEHLMANN, *Surface Crouzeix-Raviart element for the Bochner Laplacian equation*, PAMM, n/a, p. e202300207, <https://doi.org/10.1002/pamm.202300207>.
- [23] C. MEHLMANN, S. DANILOV, M. LOSCH, J. F. LEMIEUX, N. HUTTER, T. RICHTER, P. BLAIN, E. C. HUNKE, AND P. KORN, *Simulating Linear Kinematic Features in Viscous-Plastic Sea Ice models on quadrilateral and triangular Grids With Different Variable Staggering*, Journal of Advances in Modeling Earth Systems, 13 (2021), p. e2021MS002523, <https://doi.org/10.1029/2021MS00252>.
- [24] C. MEHLMANN AND O. GUTJAHR, *Discretization of Sea Ice Dynamics in the Tangent Plane to the Sphere by a CD-Grid-Type Finite Element*, Journal of Advances in Modeling Earth Systems, 14 (2022), p. e2022MS003010, <https://doi.org/10.1029/2022MS003010>.

- [25] C. MEHLMANN AND P. KORN, *Sea-ice dynamics on triangular grids*, J. Comput. Phys., 428 (2021), p. 110086, <https://doi.org/10.1016/j.jcp.2020.110086>.
- [26] I. NITSCHKE, A. VOIGT, AND J. WENSCH, *A finite element approach to incompressible two-phase flow on manifolds*, Journal of Fluid Mechanics, 708 (2012), pp. 418–438, <https://doi.org/10.1017/jfm.2012.317>.
- [27] M. OLSHANSKII, A. REUSKEN, AND A. ZHILIAKOV, *Inf-sup stability of the trace $P2$ - $P1$ Taylor-Hood elements for surface PDEs*, Mathematical Models and Methods in Applied Sciences, 32 (2022), pp. 2817–2852.
- [28] M. A. OLSHANSKII, A. QUAINI, A. REUSKEN, AND V. YUSHUTIN, *A Finite Element Method for the Surface Stokes Problem*, SIAM Journal on Scientific Computing, 40 (2018), pp. A2492–A2518, <https://doi.org/10.1137/18M1166183>.
- [29] S. REUTHER AND A. VOIGT, *Erratum: The Interplay of Curvature and Vortices in Flow on Curved Surfaces*, Multiscale Modeling & Simulation, 16 (2018), pp. 1448–1453, <https://doi.org/10.1137/18M1176464>.